ARTICLES

^{13}C NMR Line Shapes in the Study of Dynamics of Perdeuterated Methyl Groups

Piotr Bernatowicz,[†,§] Jozef Kowalewski,[*,†] Danuta Kruk,[†] and Lawrence G. Werbelow[‡]
Physical Chemistry, Arrhenius Laboratory, Stockholm University, S-106 91 Stockholm, Sweden, and Chemistry Department, New Mexico Institute of Mining and Technology, Socorro, New Mexico 87801
Received: January 12, 2004; In Final Form: July 30, 2004

Subtle features of ^{13}C NMR spectra of perdeuterated methyl groupings are discussed in detail in this work. Standard time-dependent second-order perturbation theory (WBR or Wangsness−Bloch−Redfield theory), couched in a Liouville space formalism, provides the theoretical framework for this development. It is revealed that the ^{13}C line shape is dependent upon both the scalar coupling between magnetically equivalent deuterons and deuteron autocorrelated and cross-correlated quadrupolar spectral densities. As an experimental demonstration of the presented theory, iterative line shape analyses are applied to standard ^{13}C spectra and Carr−Purcell spin−echo spectra for the ^{13}C labeled perdeuterated methyl group in DL-alanine. An activation energy for methyl rotation is determined to be 21.9 ± 1.2 kJ/mol.

Introduction

Methyl groups are ubiquitous moieties encountered not only in small organic molecules but also in large biomolecular species, whose study is of primary interest for contemporary science. Dynamics of the most abundant methyl isotopomer, $^{12}C^{1}H_3$, have been studied extensively through various ^{1}H NMR relaxation methods. Several motional models have been utilized for describing the dipolar relaxation in this spin system. The case of three spin-$^1/_2$ nuclei positioned at the vertexes of an equilateral triangle, undergoing rapid hindered rotation about a fixed axis perpendicular to the triad, is of practical importance for solid-state investigations.[1,2] Other motional models include methyl groupings attached rigidly to molecular frameworks undergoing spherical[3,4] or symmetric top[5] rotational diffusion. Numerous models that consider methyl rotations about the triad axis as well as isotropic[6] or anisotropic[7,8] diffusional motions of the triad axis itself, are particularly important for analysis of spin relaxation of the methyl moiety in isotropic media. The relevant spectral density functions derived from these models, originally applied to discussions of the longitudinal and transverse dipolar relaxation of methyl protons, can be adapted to interpret ^{13}C dipole−dipole relaxation in the $^{13}C^{1}H_3$ isotopomer.[9] The relatively simple form of these spectral densities results from the assumption of two uncorrelated motions, overall molecular tumbling (isotropic or anisotropic), and stochastic 120° methyl jumps about the C_3 (triad) axis. In practical applications, assumption of overall isotropic tumbling characterized by single correlation time is attractive when compared with anisotropic tumbling that requires five independent parameters for complete characterization. Regardless of choice of the motional model, consideration of both auto- and cross-correlated spectral densities for accurate description of relaxation processes in methyl groups is generally required.[5,8]

Perdeuterated methyl groups are not naturally abundant species. Therefore, although their dynamics were investigated by deuterium NMR long ago,[10−14] such studies did not attract much attention. However, recent interest in deuterium labeling for NMR studies of biomolecules has increased dramatically and naturally, deuterium relaxation is becoming more relevant.[15,16] The beauty of this source of information lies in the fact that ^{2}H is a spin-1 nucleus with a set of well-defined relaxation pathways. Furthermore, it offers a wider variety of relaxation parameters than its ^{1}H counterpart. For example, the full description of a collection of identical isolated deuterons requires five independent relaxation parameters[15,17] whereas a similar collection of protons is completely described by two such constants. The deuteron's electric quadrupole coupling is on the order of 100−200 kHz, which is much larger than any possible dipolar interactions involving deuterons and yet small enough to provide ^{2}H relaxation rates typically no faster than milliseconds. This is in dramatic contrast to most other quadrupolar ($I > {}^1/_2$) nuclei. Indeed, in addition to conventional deuteron relaxation parameters, other unique signatures associated with deuterium relaxation appear in resolvable multiplets of coupled nuclei.[18−28] However, when one extracts dynamical information from spectra of nuclei coupled to groups of magnetically equivalent quadrupolar nuclei (e.g., the $^{13}C^{2}H_{n>1}$ grouping), appropriate care must be taken. It has been demonstrated[28−30] that quadrupolar relaxation violates magnetic equivalence;[31] thus, scalar coupling between isochronous quadrupolar nuclei may be measured by careful observation of certain relaxation features of coupled, spin-$^1/_2$ nuclei.[32]

The present work is concerned with ^{13}C line shape analyses of completely deuterated methyl groups $^{13}C^{2}H_3$. To render this treatment useful for anticipated biodynamical investigations, only motional narrowing rather than the more stringent extreme narrowing condition is assumed. No a priori assumption regarding relative magnitudes of relaxation rates and coupling

* To whom the correspondence should be addressed. E-mail: jk@physc.su.se.
† Stockholm University.
§ On leave from Institute of Organic Chemistry, Polish Academy of Sciences, Kasprzaka 44/52, 01-224 Warsaw, Poland.
‡ New Mexico Institute of Mining and Technology.

10.1021/jp049854m CCC: $27.50 © 2004 American Chemical Society
Published on Web 09/28/2004

TABLE 1: Hilbert Space Basis Set for the $^2H_3$ Subsystem. Definitions of Labels *S*, *M*, λ, and *p* Are Given in the Text

label	description in terms of product states	$\|SM\ \lambda p\rangle$
$\|1\rangle$	$\|111\rangle$	$\|33\ A\rangle$
$\|2\rangle$	$[\|110\rangle + \|101\rangle + \|011\rangle]/3^{1/2}$	$\|32\ A\rangle$
$\|3\rangle$	$[\|11\ -1\rangle + \|1\ -11\rangle + \|-111\rangle + 2\|100\rangle + 2\|010\rangle + 2\|001\rangle]/15^{1/2}$	$\|31\ A\rangle$
$\|4\rangle$	$[\|10\ -1\rangle + \|01\ -1\rangle + \|0\ -11\rangle + \|-101\rangle + \|1\ -10\rangle + \|-110\rangle + 2\|000\rangle]/10^{1/2}$	$\|30\ A\rangle$
$\|5\rangle$	$[\|-1\ -11\rangle + \|-11\ -1\rangle + \|1\ -1\ -1\rangle + 2\|-100\rangle + 2\|0\ -10\rangle + 2\|00\ -1\rangle]/15^{1/2}$	$\|3\ -1\ A\rangle$
$\|6\rangle$	$[\|-1\ -10\rangle + \|-10\ -1\rangle + \|0\ -1\ -1\rangle]/3^{1/2}$	$\|3\ -2\ A\rangle$
$\|7\rangle$	$\|-\ 1\ -1\ -1\rangle$	$\|3\ -3\ A\rangle$
$\|8\rangle$	$[2\|110\rangle - \|101\rangle - \|011\rangle]/6^{1/2}$	$\|22\ E1\rangle$
$\|9\rangle$	$[2\|11\ -1\rangle - \|1\ -11\rangle - \|-111\rangle - 2\|001\rangle + \|010\rangle + \|100\rangle]/12^{1/2}$	$\|21\ E1\rangle$
$\|10\rangle$	$[\|10\ -1\rangle + \|01\ -1\rangle - \|0\ -11\rangle - \|-101\rangle]/2$	$\|20\ E1\rangle$
$\|11\rangle$	$[2\|00\ -1\rangle - \|0\ -10\rangle - \|-100\rangle - 2\|-1\ -11\rangle + \|-11\ -1\rangle + \|1\ -1\ -1\rangle]/12^{1/2}$	$\|2\ -1\ E1\rangle$
$\|12\rangle$	$[-2\|\ -1\ -10\rangle + \|0\ -1\ -1\rangle + \|-10\ -1\rangle]/6^{1/2}$	$\|2\ -2\ E1\rangle$
$\|13\rangle$	$[\|101\rangle - \|011\rangle]/2^{1/2}$	$\|22\ E2\rangle$
$\|14\rangle$	$[\|1\ -11\rangle - \|-111\rangle + \|100\rangle - \|010\rangle]/2$	$\|21\ E2\rangle$
$\|15\rangle$	$[2\|1\ -10\rangle - 2\|-110\rangle + \|10\ -1\rangle + \|0\ -11\rangle - \|01\ -1\rangle - \|-101\rangle]/12^{1/2}$	$\|20\ E2\rangle$
$\|16\rangle$	$[\|0\ -10\rangle - \|-100\rangle + \|1\ -1\ -1\rangle - \|-11\ -1\rangle]/2$	$\|2\ -1\ E2\rangle$
$\|17\rangle$	$[\|0\ -1\ -1\rangle - \|-10\ -1\rangle]/2^{1/2}$	$\|2\ -2\ E2\rangle$
$\|18\rangle$	$[-2\|11\ -1\rangle - 2\|1\ -11\rangle - 2\|-111\rangle + \|100\rangle + \|010\rangle + \|001\rangle]/15^{1/2}$	$\|11\ A\rangle$
$\|19\rangle$	$[\|10\ -1\rangle + \|01\ -1\rangle + \|0\ -11\rangle + \|-101\rangle + \|1\ -10\rangle + \|-110\rangle - 3\|000\rangle]/15^{1/2}$	$\|10\ A\rangle$
$\|20\rangle$	$[-2\|-1\ -11\rangle - 2\|-11\ -1\rangle - 2\|1\ -1\ -1\rangle + \|-100\rangle + \|0\ -10\rangle + \|00\ -1\rangle]/15^{1/2}$	$\|1\ -1\ A\rangle$
$\|21\rangle$	$[2\|11\ -1\rangle - \|1\ -11\rangle - \|-111\rangle + 2\|001\rangle - \|010\rangle - \|100\rangle]/12^{1/2}$	$\|11\ E1\rangle$
$\|22\rangle$	$[-2\|1\ -10\rangle - 2\|-110\rangle + \|10\ -1\rangle + \|01\ -1\rangle + \|0\ -11\rangle + \|-101\rangle]/12^{1/2}$	$\|10\ E1\rangle$
$\|23\rangle$	$[2\|00\ -1\rangle - \|0\ -10\rangle - \|-100\rangle + 2\|-1\ -11\rangle - \|-11\ -1\rangle - \|1\ -1\ -1\rangle]/12^{1/2}$	$\|1\ -1\ E1\rangle$
$\|24\rangle$	$[\|1\ -11\rangle - \|-111\rangle + \|010\rangle - \|100\rangle]/2$	$\|11\ E2\rangle$
$\|25\rangle$	$[\|01\ -1\rangle + \|0\ -11\rangle - \|-101\rangle - \|10\ -1\rangle]/2$	$\|10\ E2\rangle$
$\|26\rangle$	$[\|0\ -10\rangle - \|-100\rangle + \|-11\ -1\rangle - \|1\ -1\ -1\rangle]/2$	$\|1\ -1\ E2\rangle$
$\|27\rangle$	$[\|10\ -1\rangle + \|0\ -11\rangle + \|-110\rangle - \|01\ -1\rangle - \|-101\rangle - \|1\ -10\rangle]/6^{1/2}$	$\|00\ B\rangle$

constants is made, and full iterative numerical line shape analyses are performed.[33] Limiting scenarios are defined when appropriate.

Finally, a fundamental problem concerning application of standard Wangsness−Bloch−Redfield (WBR) relaxation theory[34] to methyl groups is revisited. The WBR theory is, by definition, semiclassical (a particle's spin is treated quantum mechanically, but spatial coordinates are considered classical). As shown recently,[35−37] such a description may fail, even in liquids at ambient temperature, for some strongly hindered CH_3 groupings. However, the nonclassical effects are expected to be less pronounced for ^2H than for ^1H substituted methyl groupings. Such belief seems justified, not only by higher deuteron mass but also, more importantly, by the good quality of "best fit" theoretical spectra presented in this work.

Theory

In the Liouville superspace formalism,[38] the intensity function, $I(\omega)$, of the NMR spectrum acquired after application of a single radio frequency pulse, is expressed by the following equation

$$I(\omega) \propto \chi^{\dagger}[\mathbf{W} - (i\omega + 2\pi\rho)\mathbf{1}]^{-1}\chi \qquad (1)$$

In the present study, we are interested only in ^{13}C spectra of the $^{13}C^2H_3$ group. Accordingly, the symbol χ in eq 1 denotes a column vector that is a Liouville representation of the ^{13}C lowering operator multiplied by the unit operator of the deuterium subsystem, $\chi \equiv \hat{I}_-(^{13}C)\hat{1}(^2H_3)$; **W** and **1** are the relevant spectral and unit supermatrices, and ρ is an empirical parameter of line broadening. In the present context, the "natural" Liouville subspace in which eq 1 is to be represented comprises 141 dimensions, each of which represents the $\hat{I}_-(^{13}C)$ operator multiplied by either one of the 27 population operators in the $^2H_3$ subsystem, or one of the 114 zero-quantum coherences possible for the latter. We note that according to the WBR theory (the use of which is implied in eq 1), relaxation-induced couplings between the dynamics of the state populations and the zero-quantum coherences are in general nonnegligible.

The average Hamiltonian of the considered system belongs to the C_{3v} symmetry point group. This fact can be exploited to reduce the dimensionality of the problem. Therefore, C_{3v} group projection operators[39] are used to obtain the (Hilbert space) basis that diagonalizes this Hamiltonian. Symmetrized states, labeled with the appropriate designation (λ = A, B, E) for the $^2H_3$ subsystem, are listed in Table 1.

Each of these states are simultaneous eigenvectors of the squared total deuteron spin, $\hat{\mathbf{S}}^2 = (\hat{\mathbf{S}}_1 + \hat{\mathbf{S}}_2 + \hat{\mathbf{S}}_3)^2$ and the z-component of total spin ($\hat{\mathbf{M}}$) operators. An additional index, *p*, is used to distinguish between states belonging to the two-dimensional representations. Each of the 27 deuteron states can be associated with one of the two basic states of spin ^{13}C, $|\alpha\rangle$, and $|\beta\rangle$.

Following a procedure described by Szymański,[40] one can demonstrate that a Liouville space symmetrized basis (brackets and parentheses are used to denote Hilbert and Liouville basis states, respectively) is spanned completely by 31 shift operators: 19 of these represent magnetic coherences and 12 represent nonmagnetic coherences (see Table 2).

The magnetic coherences involve products of $\hat{I}_-(^{13}C)$ with symmetry-adapted combinations of the population operators for the deuterium subsystem, whereas the nonmagnetic coherences refer to similar combinations with the pertinent zero-quantum coherences. The qualifications "magnetic" and "nonmagnetic" stem from the fact that the former do contribute to the observable ^{13}C magnetization (matrix elements $(k|\chi)$ are nonvanishing for the "magnetic" coherences $|1) - |19)$ whereas the latter do not ($(k|\chi) = 0$ for $k = 20, 21, ..., 31$).

The components of the vector, χ (cf. eq 1), are 1, $2^{1/2}$, and 0 for magnetic coherences obtained from Hilbert states of symmetry A and B ($|1) - |7)$, $|13) - |15)$, $|19)$), magnetic coherences obtained from Hilbert states of symmetry E ($|8) - |12)$, $|16) - |18)$), and nonmagnetic coherences ($|20) - |31)$), respectively. Inspection of Appendix 1 showing elements of the matrix **W**, calculated in the Liouville space basis defined above, reveals that the nonmagnetic coherences are sensitive to the scalar coupling between magnetically equivalent deuterons, $^2J_{DD}$.

TABLE 2: Liouville Space Basis Set for $^{13}C^2H_3$ System and Components of χ Vector

label	magnetic coherences[a]	χ	label	nonmagnetic coherences[a]	χ
|1)	$\|[\|\beta1\rangle\langle\alpha1\|]\rangle$	1	|20)	$\|[\|\beta3\rangle\langle\alpha18\|]\rangle$	0
|2)	$\|[\|\beta2\rangle\langle\alpha2\|]\rangle$	1	|21)	$\|[\|\beta18\rangle\langle\alpha3\|]\rangle$	0
|3)	$\|[\|\beta3\rangle\langle\alpha3\|]\rangle$	1	|22)	$\|[\|\beta4\rangle\langle\alpha19\|]\rangle$	0
|4)	$\|[\|\beta4\rangle\langle\alpha4\|]\rangle$	1	|23)	$\|[\|\beta19\rangle\langle\alpha4\|]\rangle$	0
|5)	$\|[\|\beta5\rangle\langle\alpha5\|]\rangle$	1	|24)	$\|[\|\beta5\rangle\langle\alpha20\|]\rangle$	0
|6)	$\|[\|\beta6\rangle\langle\alpha6\|]\rangle$	1	|25)	$\|[\|\beta20\rangle\langle\alpha5\|]\rangle$	0
|7)	$\|[\|\beta7\rangle\langle\alpha7\|]\rangle$	1	|26)	$\|[\|\beta9\rangle\langle\alpha21\| + \|\beta14\rangle\langle\alpha24\|]/2^{1/2}\rangle$	0
|8)	$\|[\|\beta8\rangle\langle\alpha8\| + \|\beta13\rangle\langle\alpha13\|]/2^{1/2}\rangle$	$2^{1/2}$	|27)	$\|[\|\beta21\rangle\langle\alpha9\| + \|\beta24\rangle\langle\alpha14\|]/2^{1/2}\rangle$	0
|9)	$\|[\|\beta9\rangle\langle\alpha9\| + \|\beta14\rangle\langle\alpha14\|]/2^{1/2}\rangle$	$2^{1/2}$	|28)	$\|[\|\beta10\rangle\langle\alpha22\| + \|\beta15\rangle\langle\alpha25\|]/2^{1/2}\rangle$	0
|10)	$\|[\|\beta10\rangle\langle\alpha10\| + \|\beta15\rangle\langle\alpha15\|]/2^{1/2}\rangle$	$2^{1/2}$	|29)	$\|[\|\beta22\rangle\langle\alpha10\| + \|\beta25\rangle\langle\alpha15\|]/2^{1/2}\rangle$	0
|11)	$\|[\|\beta11\rangle\langle\alpha11\| + \|\beta16\rangle\langle\alpha16\|]/2^{1/2}\rangle$	$2^{1/2}$	|30)	$\|[\|\beta11\rangle\langle\alpha23\| + \|\beta16\rangle\langle\alpha26\|]/2^{1/2}\rangle$	0
|12)	$\|[\|\beta12\rangle\langle\alpha12\| + \|\beta17\rangle\langle\alpha17\|]/2^{1/2}\rangle$	$2^{1/2}$	|31)	$\|[\|\beta23\rangle\langle\alpha11\| + \|\beta26\rangle\langle\alpha16\|]/2^{1/2}\rangle$	0
|13)	$\|[\|\beta18\rangle\langle\alpha18\|]\rangle$	1			
|14)	$\|[\|\beta19\rangle\langle\alpha19\|]\rangle$	1			
|15)	$\|[\|\beta20\rangle\langle\alpha20\|]\rangle$	1			
|16)	$\|[\|\beta21\rangle\langle\alpha21\|+ \|\beta24\rangle\langle\alpha24\|]/2^{1/2}\rangle$	$2^{1/2}$			
|17)	$\|[\|\beta22\rangle\langle\alpha22\|+ \|\beta25\rangle\langle\alpha25\|]/2^{1/2}\rangle$	$2^{1/2}$			
|18)	$\|[\|\beta23\rangle\langle\alpha23\|+ \|\beta26\rangle\langle\alpha26\|]/2^{1/2}\rangle$	$2^{1/2}$			
|19)	$\|[\|\beta27\rangle\langle\alpha27\|]\rangle$	1			

[a] The α and β symbols concern ^{13}C spin, and numbers following them denote Hilbert space basis states for $^2H_3$ subsystem listed in Table 1.

Likewise, the ^{13}C line shape depends on this quantity because the nonmagnetic coherences are coupled to the block of magnetic coherences by quadrupolar relaxation, similar to the case of two quadrupoles coupled to "spying" nucleus.[28−30]

Specific elements of **W** contain autocorrelated quadrupolar spectral densities,

$$J_n = \frac{3}{160}\left(\frac{e^2 q_D Q_D}{\hbar}\right)^2\left[\frac{1}{9}\frac{\tau_c}{1+(n\omega_D\tau_c)^2} + \frac{8}{9}\frac{\tau_{cl}}{1+(n\omega_D\tau_{cl})^2}\right] \quad (2)$$

and cross-correlated quadrupolar spectral densities,

$$K_n = \frac{3}{160}\left(\frac{e^2 q_D Q_D}{\hbar}\right)^2\left[\frac{1}{9}\frac{\tau_c}{1+(n\omega_D\tau_c)^2} - \frac{4}{9}\frac{\tau_{cl}}{1+(n\omega_D\tau_{cl})^2}\right] \quad (3)$$

These expressions are obtained from general formula.[6,8,41] Tetrahedral geometry and an axially symmetric electric field gradient (eq_D) collinear with the C−D bond are assumed. Other notation is considered standard. As suggested earlier, the motional model considered in eqs 2 and 3, presumes isotropic overall tumbling characterized by time constant τ_c, along with uncorrelated stochastic 120° jumps, characterized by a jump rate, $1/\tau_l$. If the jump rate is much more rapid than overall tumbling rate, then $1/\tau_{cl} = 1/\tau_l + 1/\tau_c$, can be replaced in both equations by $1/\tau_l$.

When extreme narrowing fails, the imaginary complement of eqs 2 and 3 should in principle be considered. However, they do not influence the shapes of the carbon-13 multiplet. On the other hand, it can be shown that the carbon line shape is affected by the imaginary part of the spectral density originating from cross-correlation between deuteron quadrupolar and deuteron-carbon dipolar interactions.[19−21] This results in an imaginary part of spectral densities of the form

$$L_{Q_D D_{CD}} = \frac{3\mu_0}{160\pi}(e^2 q_D Q_D)P_2(\cos\Theta_{Q_D D_{CD}})(\gamma_C\gamma_D\langle r_{CD}^{-3}\rangle) \times \left[\frac{1}{9}\frac{\omega_D\tau_c^{\,2}}{1+(\omega_D\tau_c)^2} + \frac{8}{9}\frac{\omega_D\tau_{cl}^{\,2}}{1+(\omega_D\tau_{cl})^2}\right] \quad (4)$$

These cross-correlated spectral densities appear in the anti-Hermitian part of matrix **W**, exactly as the Liouville superoperator. (Liouville superoperator, $\mathbf{L} = 1/\hbar\,(H_0 \otimes \hat{1} - \hat{1} \otimes H_0^*)$, is a Liouville space counterpart of the static Hamiltonian, H_0, where $\hat{1}$ is the unit matrix, and the symbol "⊗" denotes direct product of matrices.). Therefore, this term is identified with a frequency shift rather than a broadening of coherence. Because of its small magnitude, it can be interpreted as a second order correction to the Liouvillian arising from the interaction between the spin system and the thermal bath. In the literature, effects of this type are often called dynamic frequency shifts (DFS).[42]

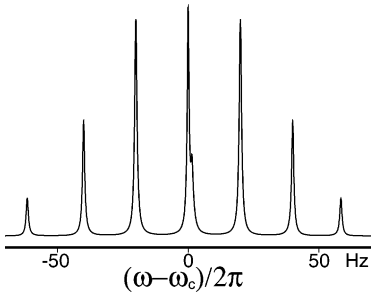

Figure 1. ^{13}C line shape at external magnetic field $B_0 = 4.7$ T, obtained under assumption of $\tau_c = 300$ ns, $\tau_l = 0.1$ ps, $^2J_{DD} = 0.1$ Hz, $^1J_{CD} = 20.0$ Hz, deuteron quadrupolar coupling of 160 kHz, deuteron-carbon dipolar coupling of 3.0 kHz, and "additional" line broadening $\rho = 0.5$ Hz. The splitting in the central line shape component is caused by dynamic frequency shifts described in the text.

Simulations

In this section, illustrative simulations of ^{13}C line shapes are presented. First, consider DFS effects that are expected to be largest for slow overall tumbling. Despite the presence of dynamic shift terms in the spectral matrix, **W**, their impact upon spectral features is negligible. For large values of τ_c, a small splitting of the central line in the carbon multiplet is apparent (Figure 1). The expected splittings of the $M = \pm 1$ components are absent. This can be understood by closer inspection of various off-diagonal matrix elements that couple pairs of magnetic coherences experiencing DFS's of the same absolute value, but opposite sign, i.e., |3) and |13). These off-diagonal elements comprise quadrupolar spectral densities sampled at zero frequency, which grow linearly along with τ_c. In the motional regime where the DFS should be apparent as distinct line splittings, the quadrupolar relaxation is fast enough to average the lines of opposite shifts. The coherences |4) and |14) are

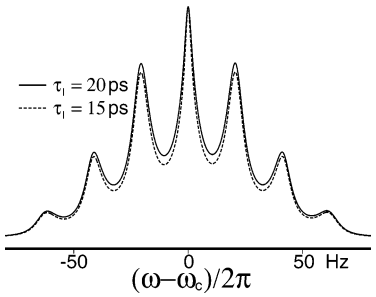

Figure 2. Standard ^{13}C spectra simulated under conditions where overall molecular tumbling is beyond extreme narrowing condition for deuteron frequency (here $\omega_D\tau_c = 1$). External magnetic field $B_0 = 9.4$ T, $\tau_c = 2.65$ ns, $^2J_{DD} = 0.1$ Hz, $^1J_{CD} = 20.0$ Hz, deuteron quadrupolar coupling of 160 kHz, deuteron-carbon dipolar coupling of 3.0 kHz, and "additional" line broadening $\rho = 0.5$ Hz were assumed. Spectra have been normalized to the same intensity of the highest line. The impact of τ_l, which is different for each of superimposed spectra, is apparent.

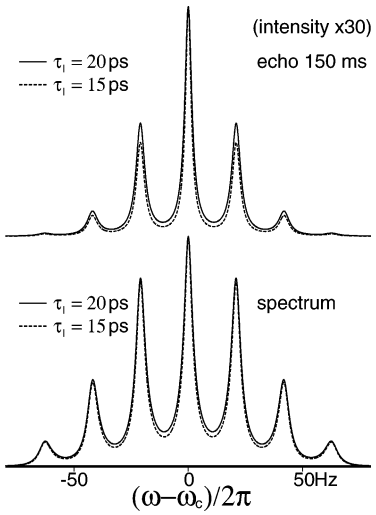

Figure 3. Comparison of simulated standard ^{13}C spectra (lower part) and Carr−Purcell spin−echoes of $\tau = 150$ ms (upper part) of the spin system discussed, under conditions where overall molecular tumbling approaches extreme narrowing condition for deuteron frequency (here $\omega_D\tau_c = 0.15$). External magnetic field $B_0 = 9.4$ T, $\tau_c = 0.4$ ns, $^2J_{DD} = 0.1$ Hz, $^1J_{CD} = 20.0$ Hz, deuteron quadrupolar coupling of 160 kHz, deuteron-carbon dipolar coupling of 3.0 kHz, and "additional" line broadening $\rho = 0.5$ Hz were assumed. Each part shows two superimposed spectra, simulated for $\tau_l = 15$ ps (dashed lines) and $\tau_l = 20$ ps (solid lines). All the spectra have been normalized to the same intensity for the highest line. A much larger discrepancy between the echo curves suggests that the Carr−Purcell pulse sequence amplifies the impact of certain parameters on the investigated line shape (with an unfortunate concomitant loss of signal-to-noise).

also coupled by zero-frequency spectral densities but they experience DFS's of the same sign, and therefore a single splitting of central line, of average magnitude $12L_{Q_DD_{CD}}$, can be recognized at extremely long τ_c.

Next, the effect of the methyl rotation rate on the line shape in the vicinity of deuteron T_1-minimum is examined. Simulations of ^{13}C spectra (Figure 2) reveal that, in this motional regime, the impact of methyl rotation rate on the line shape is significant. However, this impact is diminished when the overall molecular tumbling approaches extreme narrowing condition for ω_D (see bottom of Figure 3).

To extend the utility of line shape analysis of this spin system to a wider range of experimental conditions, a Carr-Purcell spin−echo pulse sequence, 90°−τ−180°−τ−acquisition, was used to amplify the impact of certain spectral parameters[43] (see top of Figure 3). The intensity function, $I_e(\omega)$, of ^{13}C spectrum acquired by use of this method is defined by the expression

$$I_e(\omega) \propto \chi^\dagger[\mathbf{W} - (i\omega + 2\pi\rho)\mathbf{1}]^{-1} \exp[(\mathbf{W} - (i\omega_0 + 2\pi\rho)\mathbf{1})\tau] \exp[(\mathbf{W}' - (-i\omega_0 + 2\pi\rho)\mathbf{1})\tau]\chi \quad (5)$$

where ω_0 is the transmitter frequency of the spectrometer, τ is the delay, and matrix $\mathbf{W}'$ differs from $\mathbf{W}$ by replacing ω_C (the carbon Larmor frequency) and J_{CD} (the one bond carbon-deuteron scalar coupling) with $-\omega_C$, and $-J_{CD}$, respectively. The large discrepancy between line shapes of the regular spectrum and the echo spectrum stems from the unlike evolution of particular coherences, caused by their different decay rates during τ delays.

Application of the above theoretical approach in an experimental situation is presented in following sections. Apart from the quadrupolar spectral densities, J_n and K_n, and cross-correlated dipolar-quadrupolar terms, $L_{Q_DD_{CD}}$, the impact of the other time-dependent interactions on the ^{13}C line shape has been neglected. Either their strength is relatively small, or they induce identical frequency shifts for all coherences that are nonunique in the sense that they cannot be separated from chemical shift changes induced by various inter- and intramolecular interactions.

Experimental Details

DL-Alanine-3-^{13}C-3,3,3-$^2H_3$ (**1**), selectively labeled (at least 99%) with both ^2H and ^{13}C isotopes, was purchased from ISOTEC. The saturated solution of **1** was prepared by adding 10 mg of this substance to 0.7 mL of mixture of D_2O-DMSO-d_6 in molar ratio 7:3. This sample was further used without degassing. NMR spectra were measured at temperatures 303, 283, 263, and 243 K with a Bruker AVANCE DRX 500 MHz spectrometer, and a Bruker AVANCE DRX 400 MHz spectrometer was used at 323 and 228 K. Apart from standard spectra, Carr−Purcell echoes were acquired also: of duration $\tau = 10$ ms at 228 and 243 K; 50 and 100 ms at 263 K; 30, 50, and 100 ms at 283 K; 100 and 150 ms at 303 K; and 200 ms at 323 K. Both instruments were equipped with broadband Z-gradient indirect detection probeheads and variable temperature units allowing for temperature control with accuracy of 0.1 K. Temperature calibration was carefully performed using methanol[44] within the range 303−228 K and ethylene glycol[45] at 323 K, respectively. Both the gas flow and decoupling power were carefully controlled[46] to diminish temperature gradients in the sample. Spectrometers were stabilized for at least 2 h before measurements were taken. Longitudinal relaxation time for the methyne and methyl carbons were measured at each temperature. Indirect detection[47] was used for the methyne carbon, whereas inversion−recovery[48] was used for the methyl carbon. Results obtained for the methyl carbon were used to obtain a recycle delay in Carr−Purcell experiments (always longer than 5 times the associated T_1). FIDs of about 1 s length were Fourier transformed without additional weighting or "zero-filling". A Fortran routine based on the Newton−Raphson algorithm was used to perform least-squares iterative analysis of both the standard and the echo spectra (at given temperature) simultaneously. The analysis did not comprise the convolution of NMR spectra with $\sin(\omega t_{max})/\omega t_{max}$ function arising because of finite FID acquisition time, t_{max}.[49] This effect, at relatively long $t_{max} \approx 1$ s, is assumed to be negligibly small compared with line broadenings and distortions attributed to other factors.

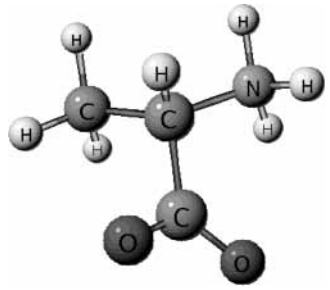

Figure 4. Neutron diffraction geometry of L-alanine in the crystal.[50]

Results and Discussion

The described theory was applied to a ^{13}C and ^{2}H labeled methyl group of **1**. To manipulate the overall reorientational correlation time, τ_c, a D_2O-DMSO-d_6 mixed solvent was utilized. Over the temperature range 263−228 K, this mixed solvent is viscous enough to place the deuterium relaxation in **1** out of extreme narrowing at moderate magnetic fields of 9.4 and 11.7 T. Although **1** belongs to a group of C_1 symmetry, it is assumed that the reorientational correlation function of the molecular framework is adequately characterized by a single exponential (time constant τ_c). Under the assumption of isotropic tumbling, τ_c can be calculated from the longitudinal relaxation rate for the α-carbon (dominated by dipole−dipole interaction with the attached proton).

Neutron diffraction geometry[50] (see Figure 4) yields the CH distance of 1.091 Å, which corresponds to dipole−dipole coupling of 23 kHz. However, it has been shown[51,52] that vibrational corrections result in a less effective CH dipolar coupling of about 21 kHz and we use this value in the analysis below. Apart from τ_c, two other parameters: the quadrupolar coupling, $(e^2q_DQ_D/\hbar)$, and scalar coupling, $^2J_{DD}$, are necessary to perform iterative line shape analysis of reasonable accuracy. A value for the quadrupolar coupling, 171 kHz, is taken from Keniry et al.[53] The scalar coupling, 0.3 Hz, is calculated from directly measured value $^2J_{HD}$, by multiplication by ratio of magnetogyric ratios of deuteron and proton, γ_D/γ_H.

The line shape analysis of the carbon-13 line shapes is performed by simultaneous least-squares fitting parameters in eqs 1−4 to the standard experimental spectra and parameters in eqs 2−5 to the Carr−Purcell echo spectra. The fitting is carried out in several different ways, denoted A−F and explained below. The analysis where all the above parameters τ_c, $(e^2q_DQ_D/\hbar)$, $^2J_{DD}$ are fixed whereas variables ω_C, $^1J_{CD}$, ρ, and τ_l are fitted simultaneously with baseline positions, intensity scaling factors and phase corrections of all the spectra, is labeled A (see Table 3 and Figure 5).

A plot of ln τ_c (calculated from spin−lattice relaxation times of α-carbon) versus 1000/T is linear over the temperature range, 323−243 K. The sudden departure from linearity at 228 K may be attributed to strong intermolecular association or the dramatic change in the macroscopic viscosity of the solvent as it approaches its freezing point. In this situation, one may expect a distribution of correlation times according to Vogel−Fulcher−Tammann model[54−56] instead of single correlation time. However, even at 228 K, the assumption of τ_c calculated from α-carbon T_1, yields a value for τ_l that fits well with the Arrhenius line in Figure 5.

The slope of ln τ_l versus 1000/T line yields an effective activation energy of 21.9 ± 1.2 kJ/mol for the methyl rotation. This value compares well with literature values collected in Table 4.

These literature values are all measured in crystalline alanine, whereas this work is the first to determine this motional parameter in the liquid state. The similarity between these values indicates that the origin of the unusually high activation energy may be different than tight crystal packing as suggested by Batchelder et al.[57] Examples of "best fit" lines obtained as the result of analysis A, superimposed with corresponding experimental spectra, are shown in Figure 6.

If the assumption of isotropic motion is flawed, then the effective correlation time experienced by the CH vector may be different than the C_3 axis of methyl group. To judge how small deviations from overall motional isotropy would affect the results of analysis A, two analyses similar to A were performed. Values of τ_c 10% larger or smaller than obtained from relaxation of α-carbon were input into the analysis. The

TABLE 3: Results of the ^{13}C Line Shape Analysis[a]

fit version	ρ (Hz)	τ_c (ps)	τ_l (ps)
	$T = 323$ K		
A	1.90 ± 0.20	29.6	2.3 ± 2.3
B	1.84 ± 0.21	29.6	3.0 ± 2.6
C	1.86 ± 0.24	10 ± 20	10 ± 20
	$T = 303$ K		
A	1.69 ± 0.09	51.3	5.0 ± 1.1
B	1.35 ± 0.10	51.3	9.3 ± 1.3
C	2.49 ± 0.08	7 ± 10	1.6 ± 2.1
	$T = 283$ K		
A	1.54 ± 0.07	102.8	8.3 ± 0.7
B	1.04 ± 0.08	102.8	13.9 ± 1.1
C	2.83 ± 0.06	18 ± 9	3.7 ± 1.8
	$T = 263$ K		
A	0.53 ± 0.07	226.6	20.2 ± 0.8
B	0.11 ± 0.09	226.6	24.3 ± 1.1
C	2.42 ± 0.06	71 ± 12	19.0 ± 3.4
	$T = 243$ K		
A	0.99 ± 0.13	634.0	32.2 ± 1.4
B	0.86 ± 0.14	634.0	32.0 ± 1.4
C	1.69 ± 0.13	340.0 ± 20	48.4 ± 3.2
	$T = 228$ K		
A	0.36 ± 0.12	5112	84.1 ± 1.3
B	−0.63 ± 0.12	5112	91.7 ± 1.2
C	0.65 ± 0.14	1370 ± 110	69.1 ± 1.9

[a] See text for explanation about individual "fit version" labels.

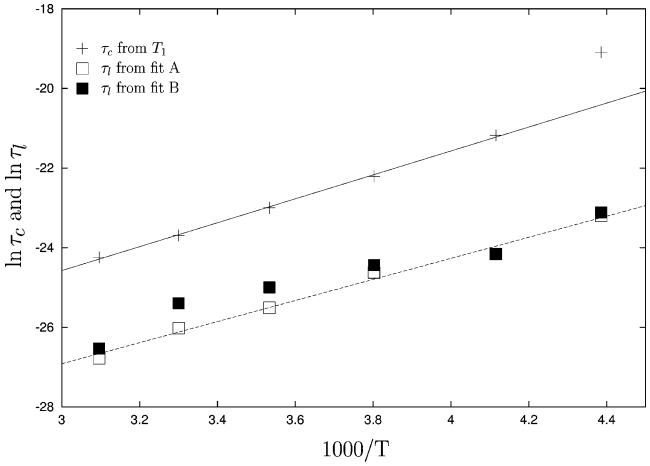

Figure 5. Dependence of ln τ_c and ln τ_l on 1000/T. Values of τ_c on this figure are calculated from longitudinal relaxation of α-carbon. Values of τ_l are obtained by iterative fitting routine in analyses *A* and *B* (see Table 3 and text). The Arrhenius activation energy calculated from slopes of above linear fits is 21.9 ± 1.2 kJ/mol and 25.0 ± 0.5 kJ/mol for methyl rotation and molecular tumbling, respectively. The points (filled squares) for large magnitude of $^2J_{DD}$ = 10000 Hz (rendering nonmagnetic coherences nonsecular) are not fitted with straight line. They are included to demonstrate the influence of these coherences on extracted values of τ_l.

TABLE 4: Literature Values of Methyl Rotation Barrier, E_a, for Zwitterionic Alanine, Alanine Hydrochloride, and Alanine Radical

E_a (kJ/mol)	reference	method
23.41	Lehmann et al.[50]	neutron diffraction of zwitterion in crystal
22.60	Batchelder et al.[57]	NMR ^{2}H relaxation of zwitterion in crystal
22.40	Andrew et al.[58]	NMR ^{1}H relaxation of zwitterion in crystal
22.00	Keniry et al.[53]	NMR ^{2}H relaxation of zwitterion in crystal
above 19.3	Detken et al.[59]	NMR ^{13}C spectra of zwitterion in single crystal
12.50	Keniry et al.[53]	NMR ^{2}H relaxation of alanine hydrochloride in crystal
17.37	Lemanov et al.[60]	ESR of radical in crystal
15.44	Miyagawa et al.[61]	ESR of radical in crystal

discrepancy of τ_l resulting from such 20% difference of assumed τ_c, varied from about 30% at 323 K down to 3% at 243 K and 7% at 228 K. Methyl activation energies extracted from these data were 21.3 ± 1.2 and 22.6 ± 1.0 kJ/mol, respectively.

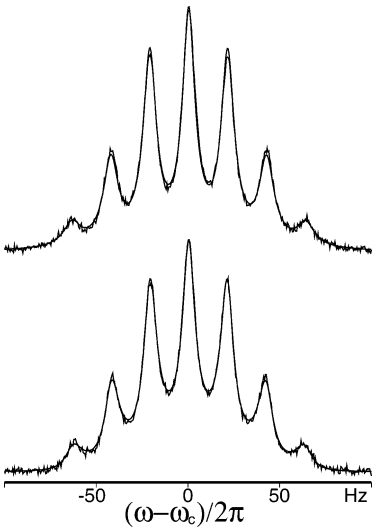

Figure 6. ^{13}C NMR experimental spectrum (bottom) and Carr-Purcell spin−echo of τ = 10 ms (top) superimposed with "best fit" lines obtained in the course of analysis A. Data acquired at B_0 = 11.7 T and T = 243 K.

Analysis B differs from A by choosing a fixed magnitude of $^2J_{DD}$ that is unrealistically large. Hence, all nonmagnetic coherences are rendered nonsecular. The impact of $^2J_{DD}$ on the extracted value of τ_l can be evaluated by direct comparison of A with B (see Figure 5).

Analysis B yields methyl activation energy 19.1 ± 2.4 kJ/mol, which is quite similar to this of case A. Despite this similarity, individual values of τ_l appear distorted if nonmagnetic coherences are ignored. Moreover, analysis B yields a nonphysical magnitude for the "additional" line broadening factor, ρ, at 228 K. Magnitudes of the standard errors listed in Table 3 grow with temperature in both the A and B cases. This shows that in vicinity of T_1 minimum, where quadrupolar relaxation dominates other broadening factors, the ^{13}C line shape is more informative than near extreme narrowing, where "additional" line broadening, ρ, is comparable to relaxation effects. Table 5 lists the specific values for the frequency-dependent spectral densities determined in this work.

In the course of analysis C, τ_l, and ρ were fitted simultaneously with τ_c (in contrast to analysis A where τ_c was kept fixed) to check if the results obtained are reliable in the absence of supplemental knowledge about molecular tumbling acquired from other sources. At first glance, the results of C are reasonable in the sense that at all temperatures "best fit" values make physical sense and have acceptable precision. However, both the activation energy for overall tumbling, 39.6 ± 2.2 kJ/mol, and methyl rotation, 27.9 ± 5.1 kJ/mol, obtained from Arrhenius plots (after rejecting point for 323 K, which suffers extremely high standard errors for both τ_c and τ_l) are different than these obtained from analysis A (cf. caption to Figure 5). Moreover, the barrier for methyl rotation yielded by C is much higher than most of the experimental values in Table 4 and has significantly larger standard error than value provided by fit A. It is recognized that method C is not reliable.

TABLE 5: Temperature Dependence J_n and K_n (Values in ms^{-1}), Extracted from Analysis A

	323 K	303 K	283 K	263 K	243 K	228 K
J_0	2.9	5.3	10.0	22.9	53.6	351.8
J_1	2.9	5.3	10.0	22.7	50.3	104.0
J_2	2.9	5.3	10.0	22.2	43.0	59.0
K_0	1.3	2.0	4.4	9.3	31.2	291.2
K_1	1.3	2.0	4.4	9.1	27.9	43.5
K_2	1.3	2.0	4.3	8.6	20.6	−1.3

Additional analyses (D and E) were performed but are not included in Table 3. These additional fits were similar to fits A and C, respectively, with artificially zeroed quadrupolar cross-correlated spectral densities, K_n. Neglect of these quantities results in a very different dynamic characterization. Version E yielded values of both correlation times with ridiculously large standard error (at 323, 303, 283, and 263 K) or nonphysical, negative values of ρ accompanied by very large standard errors of other fitted parameters (at 243 and 228 K). Version D affords, in turn, either nonphysical (at 323, 303, and 283 K) or strongly biased compared to version A (at 263 K) magnitudes of τ_l in the extreme narrowing regime and its vicinity. At some other conditions (i.e., 243 and 228 K) the deduced value of τ_l is close to that of fit A. It is difficult to confirm whether this similarity is simply accidental.

Finally, an analysis (analysis F) using only nonecho spectra was performed to see if one can use only the standard spectra and neglect echo spectra. This would save experimental time used for acquisition of low-sensitivity Carr-Purcell echoes. At most temperatures, analysis F yielded values of τ_l that were nonphysical, and "additional" line broadenings that were unreasonably high.

Conclusions

Iterative NMR line shape analysis based on WBR line shape theory and motional models derived by Woessner and Hubbard[6,8] appears to be useful tool for analysis of the dynamics of deuterated, ^{13}C-enriched methyl groupings. As expected, the results are more accurate when extreme narrowing fails. To obtain reliable results, independent determination of τ_c and $^2J_{DD}$ is required. An experimental example of application of this method was a solution of DL-alanine, where activation energy for methyl rotation was estimated to be 21.9 ± 1.2 kJ/mol.

Acknowledgment. This work was supported by the Swedish Research Council, Wenner-Gren Foundation and the Swedish Foundation for International Cooperation in Research and Higher

Education. We gratefully acknowledge stimulating discussions with S. Szymański. His generous help in the course of writing this paper was invaluable.

A. Appendix

A.1. Nonzero Real Parts of Elements of Matrix W. Since the matrix is symmetric, only elements of the upper triangle are listed. $W_{1,1} = W_{7,7} = -6*(J_1 + 2*J_2)$; $W_{1,2} = W_{6,7} = 2*(J_1 + 2*K_1)$; $W_{1,3} = W_{5,7} = 0.8*(J_2 + 2*K_2)$; $W_{1,8} = W_{7,12} = 4*(J_1 - K_1)/2^{1/2}$; $W_{1,9} = W_{7,11} = 4*(J_2 - K_2)/2^{1/2}$; $W_{1,13} = W_{7,15} = 3.2*(J_2 + 2*K_2)$; $W_{1,16} = W_{7,18} = 4*(J_2 - K_2)/2^{1/2}$; $W_{1,20} = W_{1,21} = W_{7,24} = W_{7,25} = -1.6*(J_2 + 2*K_2)$; $W_{1,26} = W_{1,27} = -W_{7,30} = -W_{7,31} = 4*(J_2 - K_2)/2^{1/2}$; $W_{2,2} = W_{6,6} = -4*(J_0 - K_0 + 2*J_1 + 2*K_1 + 2*J_2)$; $W_{2,3} = W_{5,6} = 1.2*(J_1 + 2*K_1)$; $W_{2,4} = W_{4,6} = 1.6*(J_2 + 2*K_2)$; $W_{2,8} = W_{6,12} = 4*(J_0 - K_0)/2^{1/2}$; $W_{2,10} = W_{6,10} = 4*(J_2 - K_2)/2^{1/2}$; $W_{2,13} = W_{6,15} = 32/15*(J_1 + 2*K_1)$; $W_{2,14} = W_{6,14} = 16/15*(J_2 + 2*K_2)$; $W_{2,16} = W_{6,18} = 8/3*(J_1 - K_1)/2^{1/2}$; $W_{2,17} = W_{6,17} = 4/3*(J_2 - K_2)/2^{1/2}$; $W_{2,20} = W_{2,21} = W_{6,24} = W_{6,25} = 1.6*(J_1 + 2*K_1)$; $W_{2,22} = W_{2,23} = W_{6,22} = W_{6,23} = 3.2*(J_2 + 2*K_2)/6^{1/2}$; $W_{2,28} = W_{2,29} = -W_{6,28} = -W_{6,29} = 4*(J_2 - K_2)/6^{1/2}$; $W_{3,3} = W_{5,5} = -6/75*(56*J_0 - 8*K_0 + 115*J_1 + 70*J_2 + 40*K_2)$; $W_{3,4} = W_{4,5} = 0.16*(J_1 + 2*K_1)$; $W_{3,5} = 1.92*(J_2 + 2*K_2)$; $W_{3,8} = W_{5,12} = 2.4*(J_1 - K_1)/2^{1/2}$; $W_{3,9} = W_{5,11} = 1.6*(J_0 - K_0)/2^{1/2}$; $W_{3,10} = W_{5,10} = 1.6*(J_1 - K_1)/2^{1/2}$; $W_{3,11} = W_{5,9} = 2.4*(J_2 - K_2)/2^{1/2}$; $W_{3,13} = W_{5,15} = 1.28*(J_0 + 2*K_0)$; $W_{3,14} = W_{5,14} = 128/75*(J_1 + 2*K_1)$; $W_{3,15} = W_{5,13} = 16/75*(J_2 + 2*K_2)$; $W_{3,16} = W_{5,18} = 1.6*(J_0 - K_0)/2^{1/2}$; $W_{3,17} = W_{5,17} = 32/15*(J_1 - K_1)/2^{1/2}$; $W_{3,18} = W_{5,16} = 4/15*(J_2 - K_2)/2^{1/2}$; $W_{3,20} = W_{3,21} = W_{5,24} = W_{5,25} = -4/75*(7*J_0 - 31*K_0 + 15*J_1 + 75*K_1 - 30*J_2 - 60*K_2)$; $W_{3,22} = W_{3,23} = W_{5,22} = W_{5,23} = -1.28*(J_1 + 2*K_1)/6^{1/2}$; $W_{3,24} = W_{3,25} = W_{5,20} = W_{5,21} = -0.64*(J_2 + 2*K_2)$; $W_{3,26} = W_{3,27} = -W_{5,30} = -W_{5,31} = -1.6*(J_0 - K_0)/2^{1/2}$; $W_{3,28} = W_{3,29} = -W_{5,28} = -W_{5,29} = 3.2*(J_1 - K_1)/6^{1/2}$; $W_{3,30} = W_{3,31} = -W_{5,26} = -W_{5,27} = 0.8*(J_2 - K_2)/2^{1/2}$; $W_{4,4} = -0.48*(9*J_0 + 3*K_0 + 20*J_1 - 10*K_1 + 10*J_2 + 10*K_2)$; $W_{4,8} = W_{4,12} = 0.8*(J_2 - K_2)/2^{1/2}$; $W_{4,9} = W_{4,11} = 3.2*(J_1 - K_1)/2^{1/2}$; $W_{4,13} = W_{4,15} = 0.64*(J_1 + 2*K_1)$; $W_{4,14} = 1.92*(J_0 + 2*K_0)$; $W_{4,16} = W_{4,18} = 0.8*(J_1 - K_1)/2^{1/2}$; $W_{4,17} = 2.4*(J_0 - K_0)/2^{1/2}$; $W_{4,20} = W_{4,21} = W_{4,24} = W_{4,25} = -0.32*(J_1 + 2*K_1)$; $W_{4,22} = W_{4,23} = -0.48*(9*J_0 + 3*K_0 - 5*J_1 + 15*K_1 + 10*J_2 + 10*K_2)/6^{1/2}$; $W_{4,26} = W_{4,27} = -W_{4,30} = -W_{4,31} = -1.6*(J_1 - K_1)/2^{1/2}$; $W_{8,8} = W_{12,12} = -2*(J_0 - K_0 + 4*J_1 - 2*K_1 + 4*J_2)$; $W_{8,9} = W_{11,12} = 3*(J_1 - K_1)$; $W_{8,10} = W_{10,12} = 2*(J_2 - K_2)$; $W_{8,13} = W_{12,15} = 4/15*(J_1 - K_1)/2^{1/2}$; $W_{8,14} = W_{12,14} = 8/15*(J_2 - K_2)/2^{1/2}$; $W_{8,16} = W_{12,18} = 5/3*(J_1 + 1.4*K_1)$; $W_{8,17} = W_{12,17} = 10/3*(J_2 + 1.4*K_2)$; $W_{8,19} = W_{12,19} = 4*(J_2 - K_2)/2^{1/2}$; $W_{8,20} = W_{8,21} = W_{12,24} = W_{12,25} = -0.8*(J_1 - K_1)/2^{1/2}$; $W_{8,22} = W_{8,23} = W_{12,22} = W_{12,23} = 0.8*(J_2 - K_2)/3^{1/2}$; $W_{8,26} = W_{8,27} = -W_{12,30} = -W_{12,31} = -J_1 + K_1$; $W_{8,28} = W_{8,29} = -W_{12,28} = -W_{12,29} = -J_2 + K_2$; $W_{9,9} = W_{11,11} = -3.5*J_0 - 2.5*K_0 - 6*J_1 + 4*K_1 - 8*J_2 + 4*K_2$; $W_{9,10} = W_{10,11} = 0.5*(J_1 - K_1)$; $W_{9,11} = 3*(J_2 - K_2)$; $W_{9,13} = W_{11,15} = 0.4*(J_0 - K_0)/2^{1/2}$; $W_{9,14} = W_{11,14} = 2/15*(J_1 - K_1)/2^{1/2}$; $W_{9,15} = W_{11,13} = 4/15*(J_2 - K_2)/2^{1/2}$; $W_{9,16} = W_{11,18} = 2.5*(J_0 + 1.4*K_0)$; $W_{9,17} = W_{11,17} = 5/6*(J_1 + 1.4*K_1)$; $W_{9,18} = W_{11,16} = 5/3*(J_2 + 1.4*K_2)$; $W_{9,19} = W_{11,19} = 4*(J_1 - K_1)/2^{1/2}$; $W_{9,20} = W_{9,21} = W_{11,24} = W_{11,25} = 0.8*(J_0 - K_0)/2^{1/2}$; $W_{9,22} = W_{9,23} = W_{11,22} = W_{11,23} = -0.8*(J_1 - K_1)/3^{1/2}$; $W_{9,24} = W_{9,25} = W_{11,20} = W_{11,21} = -0.8*(J_2 - K_2)/2^{1/2}$; $W_{9,26} = W_{9,27} = -W_{11,30} = -W_{11,31} = 0.5*J_0 - 0.5*K_0 + J_1 - K_1 - 2*J_2 + 2*K_2$; $W_{9,28} = W_{9,29} = -W_{11,28} = -W_{11,29} = 0.5*(J_1 - K_1)/3^{1/2}$; $W_{9,30} = W_{9,31} = -W_{11,26} = -W_{11,27} = -J_2 + K_2$; $W_{10,10} = -2*(J_0 - K_0 + 3.6*J_1 + 2.4*K_1 + 4*J_2 - 4*K_2)$; $W_{10,13} = W_{10,15} = 0.4*(J_1 - K_1)/2^{1/2}$; $W_{10,16} = W_{10,18} = 2.5*(J_1 + 1.4*K_1)$; $W_{10,19} = 4*(J_0 - K_0)/2^{1/2}$; $W_{10,20} = W_{10,21} = W_{10,24} = W_{10,25} = 0.8*(J_1 - K_1)/2^{1/2}$; $W_{10,26} = W_{10,27} = -W_{10,30} = -W_{10,31} = 0.5*(J_1 - K_1)$; $W_{13,13} = W_{15,15} = -0.08*(26*J_0 + 22*K_0 + 85*J_1 + 100*K_1 + 130*J_2 + 160*K_2)$; $W_{13,14} = W_{14,15} = 2.16*(J_1 + 2*K_1)$; $W_{13,15} = 4.32*(J_2 + 2*K_2)$; $W_{13,16} = W_{15,18} = 0.4*(J_0 - K_0)/2^{1/2}$; $W_{13,17} = W_{15,17} = 1.2*(J_1 - K_1)/2^{1/2}$; $W_{13,18} = W_{15,16} = 2.4*(J_2 - K_2)/2^{1/2}$; $W_{13,20} = W_{13,21} = W_{15,24} = W_{15,25} = -4/75*(23*J_0 + K_0 + 15*J_1 + 75*K_1 - 30*J_2 - 60*K_2)$; $W_{13,22} = W_{13,23} = W_{15,22} = W_{15,23} = 2.88*(J_1 + 2*K_1)/6^{1/2}$; $W_{13,24} = W_{13,25} = W_{15,20} = W_{15,21} = -0.96*(J_2 + 2*K_2)$; $W_{13,26} = W_{13,27} = -W_{15,30} = -W_{15,31} = -0.4*(J_0 - K_0)/2^{1/2}$; $W_{13,28} = W_{13,29} = -W_{15,28} = -W_{15,29} = 1.2*(-J_1 + K_1)/6^{1/2}$; $W_{13,30} = W_{13,31} = -W_{15,26} = -W_{15,27} = -0.8*(J_2 - K_2)/2^{1/2}$; $W_{14,14} = -0.16*(22*J_0 + 14*K_0 + 65*J_1 + 80*K_1 + 20*J_2 + 20*K_2)$; $W_{14,16} = W_{14,18} = 1.2*(J_1 - K_1)/2^{1/2}$; $W_{14,17} = 1.6*(J_0 - K_0)/2^{1/2}$; $W_{14,20} = W_{14,21} = W_{14,24} = W_{14,25} = 1.92*(J_1 + 2*K_1)$; $W_{14,22} = W_{14,23} = -0.48*(J_0 - 13*K_0 - 5*J_1 + 15*K_1 + 10*J_2 + 10*K_2)/6^{1/2}$; $W_{14,26} = W_{14,27} = -W_{14,30} = -W_{14,31} = -0.4*(J_1 - K_1)/2^{1/2}$; $W_{16,16} = W_{18,18} = -3.5*J_0 - 2.5*K_0 - 8*J_1 - 2*K_1 - 8*J_2 + 4*K_2$; $W_{16,17} = W_{17,18} = 1.5*(J_1 - K_1)$; $W_{16,18} = 3*(J_2 - K_2)$; $W_{16,20} = W_{16,21} = W_{18,24} = W_{18,25} = 0.8*(J_0 - K_0)/2^{1/2}$; $W_{16,22} = W_{16,23} = W_{18,22} = W_{18,23} = 1.2*(-J_1 + K_1)/3^{1/2}$; $W_{16,24} = W_{16,25} = W_{18,20} = W_{18,21} = 0.8*(J_2 - K_2)/2^{1/2}$; $W_{16,26} = W_{16,27} = -W_{18,30} = -W_{18,31} = 0.3*J_0 - 0.3*K_0 + J_1 - K_1 - 2*J_2 + 2*K_2$; $W_{16,28} = W_{16,29} = -W_{18,28} = -W_{18,29} = 1.5*(-J_1 + K_1)/3^{1/2}$; $W_{16,30} = W_{16,31} = -W_{18,26} = -W_{18,27} = -J_2 + K_2$; $W_{17,17} = -2*(J_0 - K_0 + 4*J_1 - 2*K_1 + 4*J_2 + 4*K_2)$; $W_{17,20} = W_{17,21} = W_{17,24} = W_{17,25} = -1.6*(J_1 - K_1)/2^{1/2}$; $W_{17,22} = W_{17,23} = 2.4*(J_0 - K_0)/3^{1/2}$; $W_{17,26} = W_{17,27} = -W_{17,30} = -W_{17,31} = -0.5*(J_1 - K_1)$; $W_{19,19} = -4*(J_0 - K_0 + 2*J_1 - 2*K_1 + 2*J_2 - 2*K_2)$; $W_{20,20} = W_{21,21} = W_{24,24} = W_{25,25} = -802/225*J_0 - 254/225*K_0 - 8*J_1 - 4*K_1 - 8*J_2 - 8*K_2$; $W_{20,21} = W_{24,25} = 1.28*(J_0 + 2*K_0)$; $W_{20,22} = W_{21,23} = W_{22,24} = W_{23,25} = 1.44*(-J_1 - 2*K_1)/6^{1/2}$; $W_{20,23} = W_{21,22} = W_{22,25} = W_{23,24} = 2.56*(J_1 + 2*K_1)/6^{1/2}$; $W_{20,24} = W_{21,25} = 2.88*(J_2 + 2*K_2)$; $W_{20,25} = W_{21,24} = 16/75*(J_2 + 2*K_2)$; $W_{20,26} = W_{20,27} = W_{21,26} = W_{21,27} = -W_{24,30} = -W_{24,31} = -W_{25,30} = -W_{25,31} = -0.8*(J_0 - K_0)/2^{1/2}$; $W_{20,28} = W_{21,29} = -W_{24,28} = -W_{25,29} = 2.4*(-J_1 + K_1)/6^{1/2}$; $W_{20,29} = W_{21,28} = -W_{24,29} = -W_{25,28} = 1.6*(J_1 - K_1)/6^{1/2}$; $W_{20,30} = W_{21,31} = -W_{24,26} = -W_{25,27} = 2.4*(J_2 - K_2)/2^{1/2}$; $W_{20,31} = W_{21,30} = -W_{24,27} = -W_{25,26} = -4/15*(J_2 - K_2)/2^{1/2}$; $W_{22,22} = W_{23,23} = -4.56*J_0 - 3.12*K_0 - 10*J_1 - 4*K_1 - 4*J_2 - 4*K_2$; $W_{22,23} = 1.92*(J_0 + 2*K_0)$; $W_{22,26} = W_{23,27} = -W_{22,30} = -W_{23,31} = 2.4*(J_1 - K_1)/3^{1/2}$; $W_{22,27} = W_{23,26} = -W_{22,31} = -W_{23,30} = 0.4*(J_1 - K_1)/3^{1/2}$; $W_{26,26} = W_{27,27} = W_{30,30} = W_{31,31} = -3.5*J_0 - 2.5*K_0 - 7*J_1 + K_1 - 8*J_2 + 4*K_2$; $W_{26,27} = W_{30,31} = 2.5*(J_0 + 1.4*K_0)$; $W_{26,28} = W_{27,29} = W_{28,30} = W_{29,31} = 1.5*(-J_1 + K_1)/3^{1/2}$; $W_{26,29} = W_{27,28} = W_{28,31} = W_{29,30} = 2.5*(J_1 + 1.4*K_1)/3^{1/2}$; $W_{26,30} = W_{27,31} = -3*(J_2 - K_2)$; $W_{26,31} = W_{27,30} = -5/3*(J_2 + 1.4*K_2)$; $W_{28,28} = W_{29,29} = -6*J_0 + 6*K_0 - 7.6*J_1 - 0.4*K_1 - 8*J_2$.

A.2. Nonzero Imaginary Parts of Elements of Matrix W. $W_{1,1} = \omega_C - 3*2\pi J_{CD} + 12*L_{Q_DD_{CD}}$; $W_{2,2} = \omega_C - 2*2\pi J_{CD}$; $W_{3,3} = \omega_C - 2\pi J_{CD} - 7.2*L_{Q_DD_{CD}}$; $W_{4,4} = \omega_C - 9.6*L_{Q_DD_{CD}}$; $W_{5,5} = \omega_C + 2\pi J_{CD} - 7.2*L_{Q_DD_{CD}}$; $W_{6,6} = \omega_C + 2*2\pi J_{CD}$; $W_{7,7} = \omega_C + 3*2\pi J_{CD} + 12*L_{Q_DD_{CD}}$; $W_{8,8} = \omega_C - 2*2\pi J_{CD}$; $W_{9,9} = \omega_C - 2\pi J_{CD}$; $W_{10,10} = \omega_C$; $W_{11,11} = \omega_C + 2\pi J_{CD}$; $W_{12,12} = \omega_C + 2*2\pi J_{CD}$; $W_{13,13} = \omega_C - 2\pi J_{CD} + 7.2*L_{Q_DD_{CD}}$; $W_{14,14} = \omega_C - 14.4*L_{Q_DD_{CD}}$; $W_{15,15} = \omega_C + 2\pi J_{CD} + 7.2*L_{Q_DD_{CD}}$; $W_{16,16} = \omega_C - 2\pi J_{CD}$; $W_{17,17} = \omega_C$; $W_{18,18} = \omega_C + 2\pi J_{CD}$; $W_{19,19} = \omega_C$; $W_{20,20} = \omega_C - 2\pi J_{CD} - 2.6*2\pi J_{DD}$; $W_{21,21} = \omega_C - 2\pi J_{CD} + 2.6*2\pi J_{DD}$; $W_{22,22} = \omega_C - 4.2*2\pi J_{DD} - 12*L_{Q_DD_{CD}}$; $W_{23,23} = \omega_C + 4.2*2\pi J_{DD} - 12*L_{Q_DD_{CD}}$; $W_{24,24} = \omega_C + 2\pi J_{CD} -$

$2.6*2\pi J_{DD}$; $W_{25,25} = \omega_C + 2\pi J_{CD} + 2.6*2\pi J_{DD}$; $W_{26,26} = \omega_C - 2\pi J_{CD} - 2*2\pi J_{DD}$; $W_{27,27} = \omega_C - 2\pi J_{CD} + 2*2\pi J_{DD}$; $W_{28,28} = \omega_C + 2*2\pi J_{DD}$; $W_{29,29} = \omega_C - 2*2\pi J_{DD}$; $W_{30,30} = \omega_C + 2\pi J_{CD} - 2*2\pi J_{DD}$; $W_{31,31} = \omega_C + 2\pi J_{CD} + 2*2\pi J_{DD}$.

References and Notes

(1) Runnels, L. K. *Phys. Rev.* **1964**, *134*, A28.
(2) Hilt, R. L.; Hubbard, P. S. *Phys. Rev.* **1964**, *134*, A392.
(3) Hubbard, P. S. *Phys. Rev.* **1958**, *109*, 1153; **1958**, *111*, 1746.
(4) Richards, P. M. *Phys. Rev.* **1963**, *132*, 27.
(5) Hubbard, P. S. *J. Chem. Phys.* **1969**, *51*, 1647.
(6) Woessner, D. E. *J. Chem. Phys.* **1962**, *36*, 1.
(7) Ivanov, E. N. *Zh. Eksp. Teor. Fiz.* **1963**, *45*, 1509.
(8) Hubbard, P. S. *J. Chem. Phys.* **1970**, *52*, 563.
(9) Ericsson, A.; Kowalewski, J.; Liljefors, T.; Stilbs, P. *J. Magn. Reson.* **1980**, *38*, 9.
(10) Ericsson, A.; Kowalewski, J. *Chem. Phys.* **1981**, *60*, 387.
(11) Bopp, T. T. *J. Chem. Phys.* **1967**, *47*, 3621.
(12) Huntress, W. T. *J. Phys. Chem.* **1969**, *73*, 103.
(13) Wallach, D.; Huntress, W. T. *J. Chem. Phys.* **1969**, *50*, 1219.
(14) Huntress, W. T. *Adv. Magn. Reson.* **1970**, *4*, 1.
(15) Millet, O.; Muhandiram, D. R.; Skrynnikov, N. R.; Kay, L. E. *J. Am. Chem. Soc.* **2002**, *124*, 6439.
(16) Skrynnikov, N. R.; Millet, O.; Kay, L. E. *J. Am. Chem. Soc.* **2002**, *124*, 6449.
(17) Werbelow, L. G. In *Encyclopedia of Nuclear Magnetic Resonance*; Grant, D. M., Harris, R. K., Eds.; Wiley: Chichester, U.K., 1996; p 4092.
(18) Martin, J. F.; Vold, R. L.; Vold, R. R. *J. Magn. Reson.* **1996**, *51*, 164.
(19) London, R. E.; LeMaster, D. M.; Werbelow, L. G. *J. Am. Chem. Soc.* **1994**, *116*, 8400.
(20) Grzesiek, S.; Bax, A. *J. Am. Chem. Soc.* **1994**, *116*, 10196.
(21) Werbelow, L. G.; London, R. E. *J. Chem. Phys.* **1995**, *102*, 5181.
(22) (a) Smith, S. A.; Murali, N. *J. Magn. Reson.* **1999**, *136*, 27. (b) Murali, N.; Nageswara Rao, B. D. *J. Magn. Reson. Ser. A* **1996**, *118*, 202.
(23) Werbelow, L. G.; London, R. E. *Concepts Magn. Reson.* **1996**, *8*, 325.
(24) Werbelow, L. G. *J. Magn. Reson.* **1986**, *67*, 66.
(25) Vold, R. L.; Vold, R. R.; Poupko, R.; Bodenhausen, G. *J. Magn. Reson.* **1980**, *38*, 141.
(26) Werbelow, L. G.; Morris, G. A.; Kumar, P.; Kowalewski, J. *J. Magn. Reson.* **1999**, *140*, 1.
(27) Bernatowicz, P.; Kruk, D.; Kowalewski, J.; Werbelow, L. G. *ChemPhysChem* **2002**, *3*, 933.
(28) Bernatowicz, P.; Szymański, S. *J. Magn. Reson.* **2001**, *148*, 455.
(29) Szymański, S. *J. Magn. Reson.* **1997**, *127*, 199.
(30) Bernatowicz, P.; Bjørlo, O.; Mørkved, E. H.; Szymański, S. *J. Magn. Reson.* **2000**, *145*, 152.
(31) Corio, P. L. *Structure of High-Resolution NMR Spectra*; Academic Press: New York, 1966, Chapter 5.
(32) Bernatowicz, P.; Szymański, S. *Mol. Phys.* **2003**, *101*, 353.
(33) Abragam, A. *The Principles of Nuclear Magnetism*; Oxford University Press: Oxford, U.K., 1961; Chapter 8.
(34) Wangsness, R. K.; Bloch, F. *Phys. Rev.* **1953**, *89*, 728. Bloch, F. *Phys. Rev.* **1956**, *102*, 104. Bloch, F. *Phys. Rev.* **1957**, *105*, 1206. Redfield, A. G. *IBM J. Res. Dev.* **1957**, *1*, 19. Redfield, A. G. *Adv. Magn. Reson.* **1965**, *1*, 1.
(35) Szymański S. *J. Chem. Phys.* **1999**, *111*, 288.
(36) Bernatowicz, P.; Szymański, S. *Phys. Rev. Lett.* **2002**, *89*, Art. No. 023004.
(37) Czerski, I.; Bernatowicz, P.; Jaźwinski, J.; Szymański, S. *J. Chem. Phys.* **2003**, *118*, 7157.
(38) Jeener, J. *Adv. Magn. Reson.* **1982**, *10*, 1.
(39) Corio, P. L. *Structure of High-Resolution NMR Spectra*; Academic Press: New York, 1966; Chapter 8.
(40) Szymański, S.; Gryff-Keller, A. M.; Binsch, G. *J. Magn. Reson.* **1986**, *68*, 399.
(41) Werbelow L. G.; Grant, D. M. *Can. J. Chem.* **1977**, *55*, 1558.
(42) Werbelow, L. G. In *Encyclopedia of Nuclear Magnetic Resonance*; Grant, D. M., Harris, R. K., Eds.; Wiley: Chichester, 1996; p. 1776.
(43) Bernatowicz, P.; Szymański, S.; Wrackmeyer, B. *J. Phys. Chem. A* **2001**, *105*, 6414.
(44) Van Geet, A. L. *Anal. Chem.* **1970**, *42*, 679.
(45) Van Geet, A. L. *Anal. Chem.* **1968**, *40*, 2227.
(46) Loening, N. M.; Keeler, J. *J. Magn. Reson.* **2002**, *159*, 55.
(47) Skelton, N. J.; Palmer, A. G., III; Akke, M.; Kördel, J.; Rance, M.; Chazin, W. J. *J. Magn. Reson.* **1993**, *102*, 253.
(48) Vold, R. L.; Waugh, J. S.; Klein, M. P.; Phelps, D. E. *J. Chem. Phys.* **1968**, *48*, 3831.
(49) Ernst, R. R.; Bodenahusen, G.; Wokaun, A. *Principles of Nuclear Magnetic Resonance in One and Two Dimensions*; Clarendon Press: Oxford, 1987; Chapter 4.
(50) Lehmann, M. S.; Koetzle, T. F.; Hamilton, W. C. *J. Am. Chem. Soc.* **1972**, *94*, 2657.
(51) Kowalewski, J.; Effemey, M.; Jokisaari, J. *J. Magn. Reson.* **2002**, *157*, 171.
(52) Henry, E. R.; Szabo, A. *J. Chem. Phys.* **1985**, *82*, 4753.
(53) Keniry, M. A.; Kintanar, A.; Smith, R. L.; Gutowsky, H. S.; Oldfield, E. *Biochemistry* **1984**, *23*, 288.
(54) Vogel, H. *Phys. Z.* **1921**, *22*, 645.
(55) Fulcher, G. S. *J. Am. Ceram. Soc.* **1925**, *8*, 339.
(56) Tammann, G.; Hesse, W. *Z. Anorg. Allg. Chem.* **1926**, *156*, 245.
(57) Batchelder, L. S.; Niu, C. H.; Torchia, D. A. *J. Am. Chem. Soc.* **1983**, *105*, 2228.
(58) Andrew, E. R.; Hinshaw, W. S.; Hutchins, M. G.; Sjöblom, R. O.; Canepa, P. C. *Mol. Phys.* **1976**, *32*, 795.
(59) Detken, A.; Zimmermann, H.; Haeberlen, U. *Mol. Phys.* **1999**, *96*, 927.
(60) Lemanov, V. V.; Sochava, L. S. *Phys. Solid State* **2003**, *45*, 1455.
(61) Miyagawa, I.; Itoh, K. *J. Chem. Phys.* **1962**, *36*, 2157.